Static and dynamic length scales in a simple glassy plaquette model

Robert L. Jack,[1] Ludovic Berthier,[2] and Juan P. Garrahan[3]
[1]*Rudolf Peierls Centre for Theoretical Physics, University of Oxford, 1 Keble Road, Oxford, OX1 3NP, United Kingdom*
[2]*Laboratoire des Colloïdes, Verres et Nanomatériaux, Université Montpellier II and UMR 5587 CNRS, 34095 Montpellier Cedex 5, France*
[3]*School of Physics and Astronomy, University of Nottingham, Nottingham, NG7 2RD, United Kingdom*
(Received 4 February 2005; revised manuscript received 6 April 2005; published 5 July 2005)

We study static and dynamic spatial correlations in a two-dimensional spin model with four-body plaquette interactions and standard Glauber dynamics by means of analytic arguments and Monte Carlo simulations. We study in detail the dynamical behavior which becomes glassy at low temperatures, due to the emergence of effective kinetic constraints in a dual representation where spins are mapped to plaquette variables. We study the interplay between nontrivial static correlations of the spins and the dynamic "four-point" correlations usually studied in the context of supercooled liquids. We show that slow dynamics is spatially heterogeneous due to the presence of diverging length scales and scaling, as is also found in kinetically constrained models. This analogy is illustrated by a comparative study of a froth model where the kinetic constraints are imposed.

DOI: 10.1103/PhysRevE.72.016103 PACS number(s): 64.60.Cn, 47.20.Bp, 47.54.+r, 05.45.−a

I. INTRODUCTION

Recently there has been considerable interest in the extent to which the slow dynamics of glass-forming liquids may be understood as a result of constraints on the kinetic properties of a system, rather than on its thermodynamics [1–3]. It has been shown that kinetically constrained models with trivial thermodynamic properties [4–6] show a slowing down at low temperature, accompanied by the stretched exponential relaxation and dynamically heterogeneous behavior characteristic of glass formers. The diverging time scales arise from dynamical fixed points at zero temperature [7,8], associated with diverging dynamical length scales.

However the only degrees of freedom in these models are phenomenological "mobility fields" [9]. Excitations in the mobility field represent regions of the glass-former where motion is possible. Presumably the energy barriers that prevent relaxation in the system are smaller than average in these regions, but there remain questions as to how these degrees of freedom are related to other physical properties of the glass-forming systems. In particular, is local mobility associated with some (possibly complicated) local static ordering? Is it always necessary to consider dynamic correlators? Is a mapping from interacting particles to a mobility field feasible?

An interesting class of models in which mobility fields emerge naturally from more familiar interacting degrees of freedom was investigated in Refs. [10,11]. In this particular case, mobile regions are associated with defects in the spin fields and these defects have a density that vanishes at zero temperature, accompanied by a divergence in the relaxation time of the system. These models therefore provide a specific, yet informative example of effective kinetic constraints arising from simple dynamical rules in conjunction with familiar Hamiltonians with multispin interactions with no quenched disorder.

In this paper we investigate correlations in the two-dimensional plaquette model [10–13]. The thermodynamic properties of the model are those of noninteracting pointlike excitations. However, when these energetic properties are combined with a simple spin-flip dynamics, the dynamical evolution at low temperatures is controlled by large energy barriers. The relaxation times diverge in an Arrhenius manner consistent with the behavior of strong glasses [14]. This is accompanied by a diverging length scale associated with dynamic correlations. Our study therefore illustrates how a mobility field might arise from a physical interacting spin system. The resulting dynamic behavior is very similar to the physics of kinetically constrained models as we show by comparatively studying a two-dimensional kinetic model inspired by the physics of covalent froths [15]. The major difference is that in the latter case dynamics is directly expressed in terms of the fundamental excitations and kinetic constraints are therefore imposed by hand. We show that the dynamical correlations in both models can be explained in terms of freely diffusing excitations.

In Sec. II we define the models, study static correlations and the representation in terms of diffusing excitations. In Sec. III we study dynamic correlations and Sec. IV contains our conclusions.

II. PLAQUETTE AND FROTH MODELS

A. The plaquette model

The Hamiltonian of the plaquette model reads [10,11]

$$H = -\frac{1}{2}\sum_{i,j=1}^{L-1} \sigma_{ij}\sigma_{i+1,j}\sigma_{i,j+1}\sigma_{i+1,j+1}, \tag{1}$$

where the $\{\sigma_{ij}\}$ are Ising spins on a two-dimensional square lattice with free boundary conditions. We specify simple spin-flip dynamics with rates given by Glauber probabilities. We denote the linear size of the lattice by L, so that there are

 ©2005 The American Physical Society

$N=L^2$ spins in the system. To demonstrate that the thermodynamic properties of this model are trivial, we make the change to plaquette variables, $\{p_{ij}\}$, defined as

$$p_{ij} = \sigma_{ij}\sigma_{i+1,j}\sigma_{i,j+1}\sigma_{i+1,j+1}. \tag{2}$$

The plaquette variables form a dual representation of the spin system. For a system with N spins, the partition sum over these N variables is equivalent to summing over $(L-1)^2$ independent plaquettes, with a final summation over $(2L-1)$ spins that lie on two orthogonal boundaries of the system.

The result is that excited plaquettes, that is those with $p_{ij}=-1$, are uncorrelated in space because the Hamiltonian becomes trivial in the plaquette representation,

$$H = -\frac{1}{2}\sum_{i,j=1}^{L-1} p_{ij}. \tag{3}$$

Excitations have a density $(e^{\beta}+1)^{-1}$ where β is the inverse temperature. Also, the free summation over boundary spins means that all states have a degeneracy of 2^{2L-1}. This arises from the symmetry of the Hamiltonian under flipping all of the spins in any row or column of the square lattice. A result of the symmetry is that only correlation functions that are invariant under this symmetry can take finite values, since there is no spontaneous symmetry breaking in this model. For example, the two-point correlator

$$\langle \sigma_{ij}\sigma_{i+x,j+y}\rangle = \delta_{x,0}\delta_{y,0}. \tag{4}$$

It is clear that this correlator must vanish if either x or y is nonzero, since flipping either row $i+x$ or column $j+y$ changes the sign of the correlation function without changing the energy of the state.

Interestingly the plaquette model also describes [16] the paramagnetic phase of the eight vertex model [17]. The additional presence of ordered states in the eight vertex model makes it a suitable analogy for a glass former with a thermodynamic melting transition. It turns out that the plaquette model remains a good description for the supercooled states below T_c, see Ref. [16].

B. Static length scales

We now discuss the aspects of the static properties of the plaquette model that are relevant to the physics of supercooled liquids and kinetically constrained models. We mentioned above that the concentration of excited plaquettes in the model is $(e^{\beta}+1)^{-1}$. The interesting behavior in the model occurs at $T<1$ (so $\beta>1$), in which these excitations are dilute. We therefore define

$$c = e^{-\beta} \ll 1. \tag{5}$$

Two typical configurations of the spins at two different low temperatures are shown in Fig. 1. It is clear that even though all two-point functions vanish by the symmetry discussed above, the system is not in a typical paramagnetic state. The axes of the underlying lattice are apparent, and their influence is felt even at relatively large length scales.

To understand static correlations we note that excited plaquettes are topological defects, in the sense that while their energy cost is localized, removing a single excited plaquette requires changes in the spin field over large distances. This is apparent from the behavior of the four-point correlation function

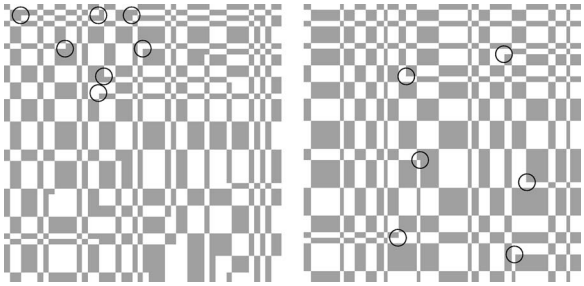

FIG. 1. Typical spin configurations at $\beta=5$ (left) and $\beta=7$ (right). At the lower temperature we identify the excited plaquettes with circles, which appear as corners in the spin field. At the higher temperature we only highlight some of the defects because they are more numerous. The smallest visible length scale is the lattice spacing. All two-point correlations vanish, even between adjacent sites.

$$C_4^{\mathrm{stat}}(x,y) = \langle \sigma_{ij}\sigma_{i+x,j}\sigma_{i,j+y}\sigma_{i+x,j+y}\rangle, \tag{6}$$

which is independent of i and j in a translationally invariant system (or sufficiently far away from the free boundaries of a finite one). We have added the superscript stat to emphasize that we consider here static correlations, as opposed to the four-point dynamic correlators studied in Sec. III. The symmetries of the Hamiltonian mean that (6) is the only nontrivial four-point function that can have a finite value. Symmetries also ensure the vanishing of all the disconnected parts of that function.

Now, the value of the combination $\sigma_{ij}\sigma_{i+x,j}\sigma_{i,j+y}\sigma_{i+x,j+y}$ is given by the parity of the number of excited plaquettes in the rectangular region defined by the four spins. To see this, we may take $x,y>0$ without loss of generality, and write

$$\sigma_{ij}\sigma_{i+x,j}\sigma_{i,j+y}\sigma_{i+x,j+y} = \prod_{x'=0}^{x-1}\prod_{y'=0}^{y-1} p_{i+x',j+y'}, \tag{7}$$

where the p_{ij} were defined in (2). This rewriting relies only on the fact that the spins are Ising variables so that $\sigma_{ij}^2=1$. The product is over all plaquettes in the rectangular region and is +1 if there is an even number of excited plaquettes and −1 if there is an odd number. Thus, if there is only one excited plaquette in the rectangle, then the product of the four spins is equal to −1, regardless of x and y. This is a signature of a topological defect.

When excited plaquettes are dilute the number of excitations in a rectangular region of area $|xy|$ is a Poissonian random variable with mean $c|xy|$. The probability that this variable takes an even value is $(1+e^{-2c|xy|})/2$. The four-point static correlator is therefore

$$C_4^{\mathrm{stat}}(x,y) = e^{-2c|xy|}, \tag{8}$$

from which one can identify the static correlation length scale $\xi_4^{\mathrm{stat}}=c^{-1/2}=e^{\beta/2}$. Physically this length scale measures the typical spacing between excited plaquettes. Clearly this

length scale diverges at $T=0$ where the concentration of defects vanishes.

It is interesting to note that in a standard kinetically constrained model where the Hamiltonian is directly expressed in terms of the relevant excitations, the distance between defects is trivially related to their concentration. In the present case, the study of simple structural correlators, e.g., two-point structure factors, does not provide information on these relevant length scales; they are only revealed when higher-order correlators are considered. More physically this means that the typical size of black and white domains in Fig. 1 does not depend on temperature while the concentration of circles does, so that by naively looking at the interacting spins one would get the wrong impression that there is no diverging length scale in the system. Taking the analogy with liquids seriously this suggests that while the structure factor of supercooled liquids shows no particular trend when temperature is decreased, higher-order correlators related to some yet unknown local ordering could reveal the presence of increasing length scales, as assumed in several scenarii of the glass transition [18–20].

The problem with the correlator (6) is that it is highly specific to the model under study, which has special symmetries. It would be more useful to define static quantities which are independent of the model under study but still reveal the presence of growing length scales. An idea is that in the presence of diverging length scales, large fluctuations can also be expected. Let us consider the two-point quantity,

$$c_2^{\mathrm{stat}}(x,y) = \frac{1}{N}\sum_{i,j=1}^{L} \sigma_{ij}\sigma_{i+x,j+y}. \tag{9}$$

where the sum is over a finite region of an infinite spin system. The number of terms in the sum is $N=L^2$; we will later take the limit of large L so as to extract a well-defined measure of the size of fluctuations.

The expectation value of c_2^{stat} is a sum of two-point correlation functions. Equation (4) therefore constrains it to vanish in the thermodynamic limit (except in the trivial case, $x=y=0$). In other words, $\langle c_2^{\mathrm{stat}}(x,y)\rangle = \delta_{x,0}\delta_{y,0}$. However, even when the expectation value of c_2^{stat} is zero, its fluctuations are not. One can therefore define the following susceptibility:

$$\chi_2^{\mathrm{stat}}(x,y) = N[\langle c_2^{\mathrm{stat}}(x,y)^2\rangle - \langle c_2^{\mathrm{stat}}(x,y)\rangle^2], \tag{10}$$

where the disconnected part in fact vanishes by symmetry [except at $x=y=0$ where it exactly cancels the connected part, so that $\chi_2^{\mathrm{stat}}(0,0)=0$]. The connected part is a sum of four-point static expectation values, but symmetries of the model constrain most of these to be zero as well. The only nonzero terms are either of the form of (6), or else trivial (for example $\langle \sigma_{ij}^2 \sigma_{i'j'}^2\rangle$). Assuming that at least one of x and y is nonzero, we write out the sums and collect the nonvanishing terms, arriving at

$$\begin{aligned}\chi_2^{\mathrm{stat}}(x,y) &= \frac{1}{N}\sum_{i,i',j,j'=1}^{L} \langle \sigma_{ij}\sigma_{i+x,j+y}\sigma_{i'j'}\sigma_{i+x,j'+y}\rangle \\ &= (1-\delta_{x,0})(1-\delta_{y,0}) + \frac{1}{N}\sum_{i,j,m=1}^{L} [\delta_{x,0}C_4^{\mathrm{stat}}(i-m,y) \\ &\quad + \delta_{y,0}C_4^{\mathrm{stat}}(x,j-m)]. \end{aligned} \tag{11}$$

We note that the first term gives a trivial value of unity for $\chi_2^{\mathrm{stat}}(x,y)$ unless at least one of x or y is equal to zero. This arises from the four-point correlators with $i=i'$ and $j=j'$; we will see shortly that $\chi_2^{\mathrm{stat}}(x,0)$ also approaches this trivial value when x becomes much longer than the relevant correlation length.

The definition of c_2^{stat} contains a dependence on the cluster size, L. However, the physically relevant limit is when L is much greater than all correlation lengths in the system; in this limit then $\chi_2^{\mathrm{stat}}(x,y)$ converges to a finite value. From (8), we can identify the sums as geometric series: taking care not to double count the terms with $i=i'$ or $j=j'$, we find that

$$\lim_{L\to\infty} \chi_2^{\mathrm{stat}}(x,0) = \sum_{y=-\infty}^{\infty} e^{-2c|xy|} = \coth(c|x|), \tag{12}$$

for $x\neq 0$. From these fluctuations we identify a second static length scale,

$$\xi_2^{\mathrm{stat}} = c^{-1} = e^{\beta}, \tag{13}$$

which also diverges at $T=0$. Physically this length scale represents the mean distance between adjacent excited plaquettes in the same row or column of the square lattice, and is therefore much greater than the typical spacing between excited plaquettes, ξ_4^{stat}.

In deriving Eq. (13) we again made use of the special symmetries of the model, which is an undesired feature of this treatment. This can be cured by noting that ξ_2^{stat} may be accessed through a circular average,

$$\chi_2^{\mathrm{stat}}(r) \equiv \int_0^{\infty} \frac{d\theta}{2\pi r}\chi^{\mathrm{stat}}(x,y) = \frac{2}{\pi r}\coth(cr) + 1, \tag{14}$$

where the integral over θ is to be understood as a sum over the integrand at values of x,y such that $r-\frac{1}{2} < \sqrt{x^2+y^2} < r+\frac{1}{2}$. Thus the length scale ξ_2^{stat} can indeed be extracted from fluctuations of two-point measurements that do not depend on knowing the exact orientation of the lattice axes or the special symmetries of the model.

To verify these exact results, we performed static Monte Carlo simulations to obtain $\chi_2^{\mathrm{stat}}(x,y)$ both for $y=0$ and for the trivial case $x,y\neq 0$ where the susceptibility takes the value unity. The results are shown in Fig. 2.

C. Inherent structures and droplets

We now discuss the above findings in relation to alternative approaches to the glass transition that involve growing length scales of a static nature. A problem with these approaches is that there exist no numerical or experimental indications for the presence of such static correlations. How-

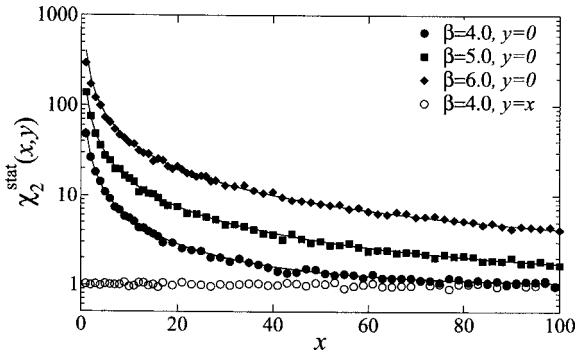

FIG. 2. Simulation data confirming the analytic results. We show χ_2^{stat} for $y=0$ at three different temperatures (filled symbols); the solid lines are the result of (12). We also show that χ_2^{stat} takes the trivial value of unity when neither x nor y is zero. We use a cluster of 10^6 spins to avoid finite size effects.

ever two recent papers have discussed methods to detect growing static length scales in supercooled liquids that we now discuss in the context of the plaquette model.

Bertin [21] suggested to consider the spatial structure of inherent structures [22] and studied a one-dimensional disordered Potts model to illustrate his ideas. The procedure is as follows. Take an equilibrium configuration of the system at finite temperature T and quench it to its inherent structure. Now fix the orientation of the spins on the boundary of a finite portion of the system of linear size ℓ. Finally, minimize the energy of the finite size system given these boundary conditions. Bertin finds that there exists a well-defined length scale, $\ell^*(T)$, which is such that it is typically possible to find a lower energy structure when $\ell > \ell^*$, while the system is already at its ground state for smaller sizes, $\ell < \ell^*$.

In the plaquette model, the effect of quenching to $T=0$ is that dimers freely diffuse (see below) until they get absorbed, and then all motion stops. The inherent structure is therefore a structure with single defects only. On quenching from equilibrium these defects will be randomly distributed in space, except that they are never on adjacent sites (since that would be a dimer). So, consider a rectangular region of the sample of linear size ℓ. We may ask, what is the probability that this region minimizes the energy, subject to its boundaries remaining fixed? Fixing the $4(\ell-1)$ spins that lie on the boundaries constrains the parity of the number of defects in each row and in each column. Thus the (possibly degenerate) ground state of the square region contains at most one defect in each row or column, according to their parities. It is then obvious that when $\ell > \ell^* \sim \xi_2^{\mathrm{stat}}$ there will typically be more than one defect in each line and column and the inherent structure will not coincide with the ground state of the finite size system. We conclude therefore that Bertin's method would successfully determine the static correlation length scale ξ_2^{stat} discussed in the preceding section. The main difference between our model and that of Bertin is that we cannot identify a tiling of inherent structures with regions that minimize the energy because our defects are pointlike objects that obviously cannot delimit a particular area.

In a real space description of the random first order transition it is imagined that above its static Kauzmann transition the system is composed of an assembly of entropic droplets [18]. Revisiting this idea Bouchaud and Biroli proposed to associate a temperature dependent length scale, $\xi^*(T)$, to these droplets in the following manner [23]. Consider an equilibrium configuration of the system at temperature T. Then consider a finite portion of the system of linear size ℓ and freeze its boundary conditions. Now let this finite size system evolve at temperature T with its boundary conditions fixed. If $\ell < \xi^*$ the system should effectively be nonergodic while dynamic correlation functions would go to zero at large times for $\ell > \xi^*$.

In the plaquette model this procedure was studied from a different perspective in Ref. [13] where the thermodynamics of finite size systems was computed exactly for a particular choice of boundary conditions. It was found that in a finite size system there indeed exists a glass transition temperature, which is manifested by a downward jump in the specific heat which shifts to lower temperature for larger ℓ. Although this calculation is not exactly the procedure described by Bouchaud and Biroli where any sort of boundary conditions should be studied, it is very close in spirit. Physically, the nonergodic behavior is due to the fact that when ℓ is too small the system cannot rearrange without altering its boundaries. This happens as above when lines or columns only contain one or no defect, i.e., when $\ell < \xi_2^{\mathrm{stat}}$ and we conclude that the procedure of Ref. [23] would once more yield the correct correlation length scale, $\xi^* \sim \xi_2^{\mathrm{stat}}$.

D. Diffusing excitations in the plaquette model

We now consider the dynamics of the plaquette model. The fundamental moves are spin-flips. When a single spin is flipped the states of the four plaquettes surrounding that spin must all change. Thus there are five types of move, depending on the environment of the relevant spin. If a spin has no adjacent excited plaquettes, then flipping that spin incurs an energy cost $\Delta E=4$, so these moves are suppressed by a factor c^4. Now, if a spin is adjacent to exactly one excited plaquette, then its flips cost $\Delta E=2$ and are suppressed only by a factor c^2. The density of such sites is approximately c at low temperatures, so these flips are already more significant than those involving $\Delta E=4$. Finally spins adjacent to pairs of excited plaquettes can flip without energy cost, $\Delta E=0$, and that those adjacent to three or four excited plaquettes have $\Delta E < 0$ and will therefore relax rapidly to the low energy state with one or zero excited plaquettes, respectively.

The key physical point is that excited plaquettes act as sources of mobility, since the energetic barriers to spin flips are smaller in those regions. This observation allows us to identify the excited plaquettes as the excitations in the mobility field by analogy with kinetically constrained models. The square lattice of the plaquette model has a surprising effect on the diffusion of these mobility excitations, because pairs of adjacent excited plaquettes diffuse freely, but are confined to one dimension, see Fig. 3. As shown in Refs. [12,13], this is responsible for the form of the low temperature divergence of the relaxation time, $\tau \sim c^{-3}$.

E. The froth model

We now introduce a simple model that shares many features in its dynamical behavior with the plaquette model.

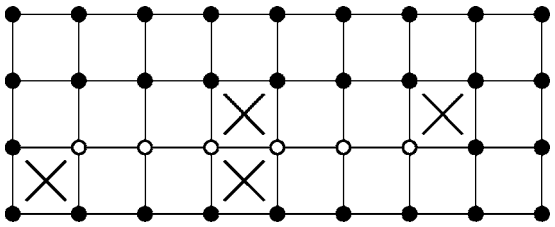

FIG. 3. Sketch of a dimer explaining the origin of the strongly anisotropic dynamical correlations in the plaquette model. Excited plaquettes are marked with a × sign. Spins are marked by small circles but the state of the spins is not shown. The dimer diffuses along the x direction with no energy barrier. Open circles mark spins that can be flipped as part of this free diffusive process. Flipping of spins marked by closed circles costs at least $\Delta E=2$.

Consider a mobility field that is defined on the plaquettes of a hexagonal lattice. Each defect carries an energy of unity, so the Hamiltonian takes the trivial form

$$H_{\text{froth}} = -\frac{1}{2}\sum_{i=1}^{N} n_i, \tag{15}$$

where there is a defect on site i if $n_i=-1$; otherwise $n_i=+1$. Dynamical moves involve flipping the values of four of the n_i on plaquettes that are related by a Feynman diagram shape, see Fig. 4. This sort of model was studied in the context of covalent froths [15], so we refer to it as the froth model in what follows. The similarity between Hamiltonians (3) and (15) is evident but the froth model does not have an equivalent spin representation.

Comparisons between the dynamics of the froth model and those of the plaquette model are instructive because the only difference between their dynamics is the structure of the underlying lattice. However, while the diffusing pairs of excitations in the plaquette model were confined to one dimension as a result of the square lattice, Fig. 3, the equivalent dimers of the froth model are free to diffuse across the whole two-dimensional plane, Fig. 4.

To first illustrate the strong effect of the choice of lattice on the dynamics we show typical realizations of the persistence function [2] of each system in Fig. 5. The persistence function on site i is defined by $b_i(t,t')=1$ if the state of that site has remained constant for all times between t' and $t+t'$, otherwise $b_i(t,t')=0$. It is clear from Fig. 5 that the effect of the square lattice is to introduce strong anisotropy into the dynamic spatial correlations. The remainder of this paper contains discussions of the dynamic correlations shown in Fig. 5.

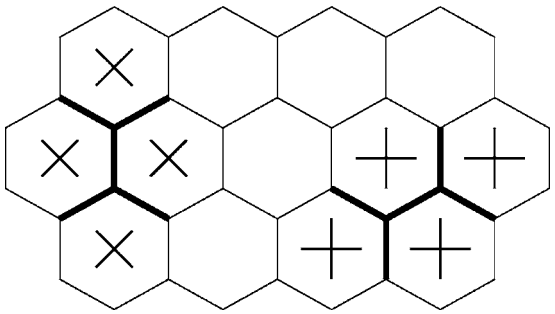

FIG. 4. Two possible moves in the froth model. The binary variables n_i are defined on the hexagons. The + and × signs mark sets of four n_i. A single move involves flipping all four of any such set. The Feynman diagram shapes are shown in bold.

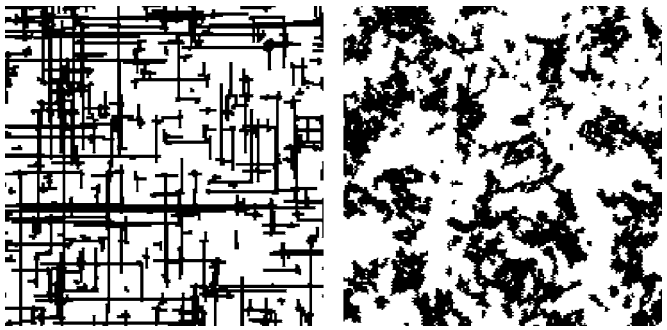

FIG. 5. Realizations of persistence function in the plaquette model (top) and the froth model (bottom). Plaquettes that have flipped between time zero and time t are coloured black. The time t is such that the fraction of black plaquettes is approximately 0.4. Both simulations are at $\beta=5$ and show regions of size 200×200. The strong anisotropy in the top panel is purely a result of the underlying square lattice in the plaquette model.

III. DYNAMIC CORRELATIONS

A. Dynamic correlations in the plaquette model

In the preceding section we introduced the persistence function to quantify dynamics in the plaquette model. This was a convenient way to compare dynamics between froth and plaquette models. However the presence of the underlying spin field in the plaquette model means that its dynamics is more naturally investigated in terms of the spin-spin autocorrelation

$$a_{ij}(t,t') = \sigma_{ij}(t')\sigma_{ij}(t'+t). \tag{16}$$

The two-time form of this operator makes it more natural than the persistence function which depends on the spin at all times between t' and $t'+t$.

A typical realisation of $a_{ij}(t,t')$ is shown in Fig. 6. The autocorrelation function retains slightly more information than the persistence function. If the system makes an excursion to an excited state before returning to its initial one, then the autocorrelation function records the fact that the overall state has not changed, but the persistence function does not. For this reason, the autocorrelation data shows the spatial correlations more clearly than the persistence data.

We now investigate the anisotropic dynamic correlations in the plaquette model more carefully. Consider the two-point, two-time (i.e., four-point) correlation function

$$\widetilde{C}_{2,2}(x,y,t) = \langle a_{ij}(t,t_0)a_{i+x,j+y}(t,t_0)\rangle - \langle a_{ij}(t,t_0)\rangle\langle a_{i+x,j+y}(t,t_0)\rangle. \tag{17}$$

In equilibrium this function is independent of (i,j,t_0) since the system is invariant under translations in both space and

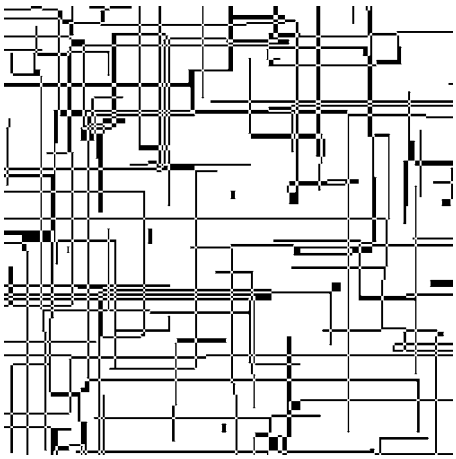

FIG. 6. Typical realisation of the autocorrelation in the plaquette model. Sites with $a_{ij}=-1$ are colored black. The inverse temperature is $\beta=5$ and the time scale is such that $\langle a_{ij}\rangle \simeq 0.6$. This figure is from the same time series as for the persistence field in Fig. 5 (top) but the time t is longer because most of the contributions to the persistence are from dimers that are reabsorbed at their emission point.

time. It is convenient to discuss also normalized correlations,

$$C_{2,2}(x,y,t) = \frac{\tilde{C}_{2,2}(x,y,t)}{1-\langle a_{ij}(t,t_0)\rangle^2}, \tag{18}$$

so that $C_{2,2}(0,0,t)=1$.

We are more particularly interested in the scaling of $C_{2,2}$ at low temperatures. We find that the scaling contains contributions from diverging length and time scales, consistent with the presence of a dynamical critical point at $T=0$. For example, the on-site autocorrelation function $\langle a_{ij}(t,t')\rangle$ obeys the scaling relation [12] $\langle a_{ij}(t,t_0)\rangle = f_1(c^3 t)$. However the spatial scaling is not as simple as this temporal relation. It is clear from Fig. 6 that the presence of the underlying square lattice is relevant to $C_{2,2}$ even at low temperatures.

We have investigated the function $C_{2,2}$ in some detail using Monte Carlo simulations with a continuous time algorithm [24]. Since there is a correlation length proportional to $1/c$ in the static properties of the system, it is necessary to use rather large system sizes. We use periodic boundary conditions, which require systems large enough that typical rows and columns of the lattice contain at least two excited plaquettes. Otherwise there are rather strong finite size effects, as observed in Ref. [13]. Typically we use system sizes of 10^6 spins. The typical error bars are of the order of the symbol sizes in the figures, except where noted otherwise. Time is measured in Monte Carlo sweeps throughout and all distances are in units of the lattice spacing.

In Fig. 7 we show the strong correlations in $C_{2,2}$ along the axes of the model, and their rapid decrease away from those axes. In order to show data at different temperatures, we use times t that scale with c^{-3} so that $\langle a_{ij}(t,t')\rangle$ is the same at each temperature. We see that the length scale associated with $C_{2,2}(x,0,t)$ grows rapidly at low temperatures while the off-axis correlations measured by $C_{2,2}(x,x,t)$ are weak and

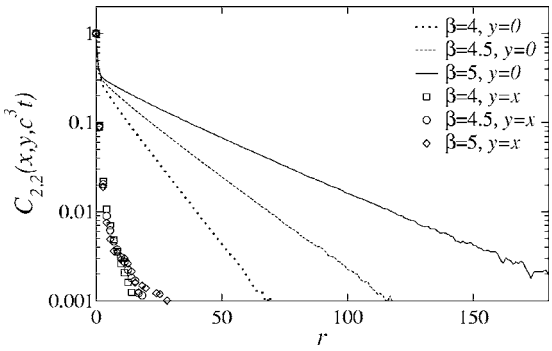

FIG. 7. Plots of $C_{2,2}(x,y,c^3t)$ with $y=0$ and with $y=x$, as a function of $r=\sqrt{x^2+y^2}$. Times are such that $c^3t=0.07$ so that $\langle a_{ij}(t,t')\rangle \simeq 0.5$. The length scale for on-axis correlations increases with decreasing temperature, but there is no scaling for the off-axis correlator.

do not depend strongly on β. In the representation of Fig. 6, $C_{2,2}(x,0,t)$ measures the typical length of the rodlike objects, which gets large at small temperatures. However, the absence of correlations away from the axes of the lattice indicates a lack of correlation between those objects. The microscopic origin of this behavior is in the one-dimensional diffusion of pairs of excited plaquettes sketched in Fig. 3.

We now consider the full time and space dependence of $C_{2,2}(x,0,t)$ in a little more detail. It is convenient to start the discussion by focusing on the corresponding dynamical four-point susceptibility [25,26]

$$\chi_{2,2}(t) = \sum_{xy} C_{2,2}(x,y,t). \tag{19}$$

This quantity is proportional both to the typical correlation area and to the strength of the correlations. From Fig. 7 we expect $C_{2,2}(x,0,t) \approx \rho(t) f[x/\xi_{2,2}(t)]$ at large x (see also below) so that we may write

$$\chi_{2,2}(t) \approx \rho(t)\xi_{2,2}(t)^{d_f}. \tag{20}$$

In this expression d_f is the fractal dimension associated with the correlations, $\xi_{2,2}(t)$ the linear size of a correlated region, $\xi_{2,2}^{d_f}$ its area and the quantity $\rho(t)$ measures the strength of the correlations. We show $\chi_{2,2}(t)$ at several temperatures in Fig. 8 (top). There are three distinct regimes in this function, a power law increase at small times; a broad maximum whose width increases with decreasing temperature; and a rapid decrease at larger times.

These data are easily interpreted in terms of the excitations described in Sec. II. At short time scales the rodlike objects shown in Fig. 6 grow in a diffusive manner. These objects have $d_f=1$, and we therefore expect $\chi_{2,2}(t) \sim (t^{1/2})^{d_f=1}$, as observed in Fig. 8. Moreover this behavior is independent of c since a pair of excited plaquettes can diffuse at no energy cost.

At larger times, dimers that have diffused can be absorbed on encountering an isolated excited plaquette, preventing further growth of the rods. The dynamic length scale therefore saturates to the mean distance between isolated defects along one direction of the square lattice. This is precisely the

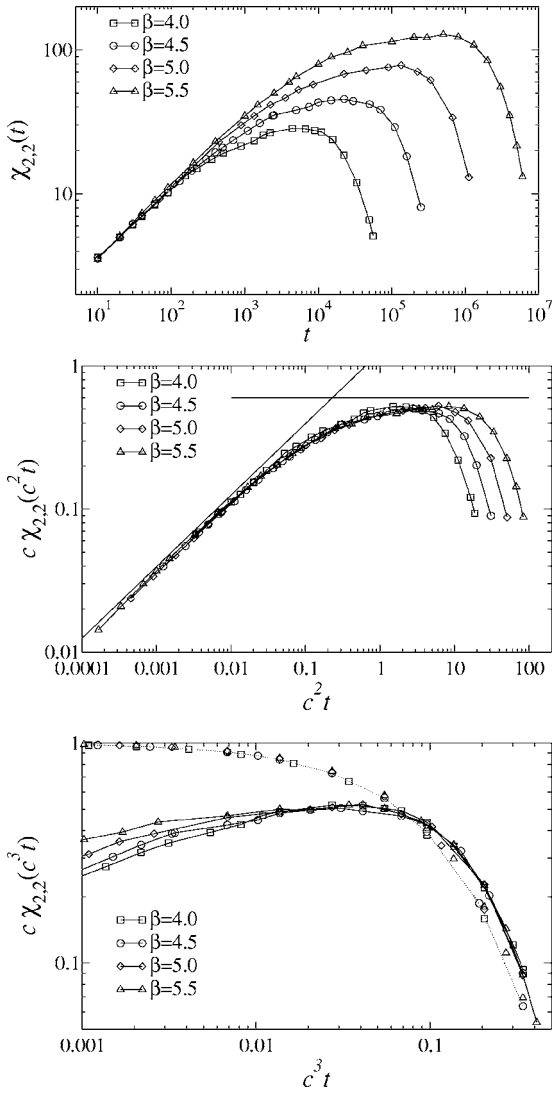

FIG. 8. Top, plots of $\chi_{2,2}(t)$ at various temperatures. Middle, rescaling of time to c^2t showing saturation at $c^2\tau_{\rm sat}\sim 1$. Lines are a power law, $t^{0.5}$, consistent with diffusive motion, and a horizontal plateau showing saturation at $c\chi_{2,2}\sim 0.6$. Bottom, rescaling of time to c^3t showing decrease of correlations due to decreasing ρ which scales in the same way as the spin-spin autocorrelation functions. (The autocorrelation functions are displayed as the data that collapse on the dotted line.)

physical content of the static length scale $\xi_2^{\rm stat}\sim c^{-1}$ discussed above. Since the process is diffusive, saturation of $\xi_{2,2}$ to $\xi_2^{\rm stat}$ takes place at a time scale given by

$$\tau_{\rm sat}\sim c^{-2}. \tag{21}$$

Saturation at time $\tau_{\rm sat}$ is observed in the numerical data, as shown in the middle frame of Fig. 8.

Finally, after saturation there is little change in the correlations until the susceptibility starts to decrease for times $t\sim c^{-3}$. Scaling in this late-time regime is governed by the time dependence of the factor $\rho(t)$ in Eq. (20) which starts to decrease significantly when the rods start to overlap. When two rods cross the site at which they intersect has flipped twice. It therefore has $a_{ij}=+1$, unlike the rest of the rod which has $a_{ij}=-1$. This effect takes place on the time scale set by the autocorrelation function, which scales as $\tau\sim c^{-3}\gg\tau_{\rm sat}$. This behavior is confirmed in the bottom panel of Fig. 8 where the scaling of $\langle a_{ij}\rangle$ is also shown.

B. Dynamic scaling in the plaquette model

We now discuss the spatial structures in $C_{2,2}(x,0,t)$, and their scaling. At small times, pairs of defects diffuse in one dimension. Dynamic correlations only depend on $x/\xi_{2,2}(t)\sim x/t^{1/2}$, and the scaling of χ is consistent with $d_f=1$. In this time regime we may identify a dynamical exponent, $z=2$. At larger times, $\tau_{\rm sat}\ll t$, the dynamical lengthscale saturates at $\xi_{2,2}(t)\sim\xi_2^{\rm stat}$. This saturation of the dynamic length scale reflects the fact that the typical distance that a dimer travels before being absorbed is given by $\xi_2^{\rm stat}$. We may identify this length as a mean free path for dimers diffusing along one-dimensional paths. Thus the structure of dynamical correlations is explained in terms of the constrained one-dimensional motion of diffusing pairs of defects. The behavior may be summarized as

$$C_{2,2}(x,0,t)=\begin{cases} f_{2a}(x^2/t), & c^2t\ll 1,\\ f_{2b}(c^3t)f_{2c}(cx), & c^2t\gg 1. \end{cases} \tag{22}$$

We illustrate this behavior in Fig. 9. The function f_{2a} is shown in the top panel, along with our theoretical prediction for it [Eq. (23), discussed below]. In the middle panel, we show the spatial correlations at various times that are all greater than the saturation time. The spatial dependence of the correlations is not changing, while their strength gets weaker and scales with the relaxation time c^{-3}. Finally, we may normalize the correlations by their spatial integral as a way to extract the scaling function $f_{2c}(cx)$ in the bottom panel of Fig. 9.

Note that these scaling plots contain no free parameters. There remain small deviations from scaling arising from the presence of the lattice at small distances and from the fact that the two time scales $\tau_{\rm sat}$ and τ are not infinitely separated. However Fig. 9 is clear evidence that the dynamical correlations are well described by independent random walkers in one dimension, with a mean lifetime of approximately $\tau_{\rm sat}$.

We may evaluate exactly the function $f_{2a}(x^2/t)$, which gives the value of $C_{2,2}(x,0,t)$ for times much smaller than the saturation time. The four spin function $a_{ij}(t,t_0)a_{i+x,j}(t,t_0)$ takes the value -1 if either (1) a dimer starts between the sites (i,j) and $(i+x,j)$ and diffuses out of that region, or (2) a dimer starts outside that region and diffuses into it, or (3) a dimer diffuses along the y direction, flipping one of the spins, or (4) some more complicated process occurs, involving two dimers or the absorption or emission of a dimer by an isolated excited plaquette.

Assuming that the dimers diffuse freely then the first three processes mentioned above are easy to analyze by manipulation of the diffusion equation in one dimension. We arrive at the following result for $C_{2,2}(x,0,t)$:

$$f_{2a}(x^2/t)=\frac{1}{2}\left[e^{-x^2/2t}-\sqrt{\pi}\frac{x}{\sqrt{2t}}\mathrm{erfc}\left(\frac{x}{\sqrt{2t}}\right)\right]+\mathcal{O}(c^2), \tag{23}$$

where $\mathrm{erfc}(x)\equiv(2/\sqrt{\pi})\int_x^\infty dy\, e^{-y^2}$.

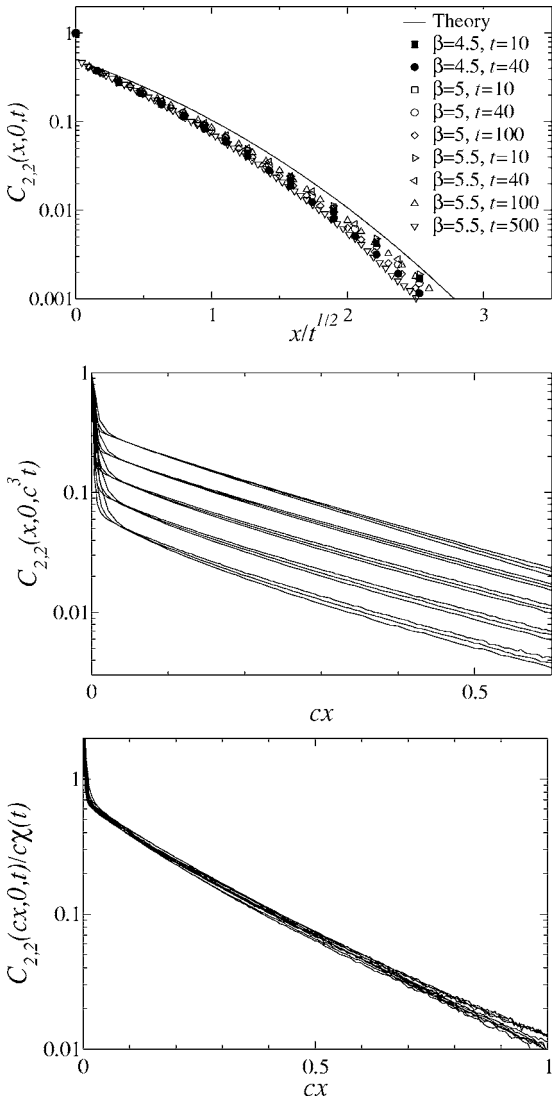

FIG. 9. Top, data collapse of $C_{2,2}(x,0,t)$ on rescaling of space by $t^{1/2}$ independently of c. The solid line is the prediction for this function, assuming free (one-dimensional) diffusion of pairs of excited plaquettes, valid for times $t \ll \tau_{\rm sat}$ [Eq. (23)]. Middle, scaling of $C_{2,2}(x,0,t)$ for $t \gg \tau_{\rm sat}$. We plot temperatures between $\beta=4$ and $\beta=5.5$ for different scaled times $c^3t=1$, 2, 3, 4, 5 (top to bottom). Errors are smaller than the distances between traces. Bottom, collapse of the data of the middle panel using $C_{2,2}(x,0,t)/[c\chi_{2,2}(t)]$ showing the scaling function $f_{2c}(x)$ in Eq. (22).

In deriving this result we assumed that only dimers present at $t=t_0$ affect the spins, and that these dimers diffuse freely throughout the system. This assumption breaks down when the dimers present in the initial state start to encounter isolated defects, where they are absorbed. This is the physics behind the collapse in the middle panel of Fig. 8; and happens when c^2t reaches a value of order unity. The absorption of the dimers cuts off the growth of the dynamical length scale, leading to shorter range correlations than those predicted, as is visible from the top panel of Fig. 9. In particular, we note that the correspondence between theory and simulation is best for small times (compared to $\tau_{\rm sat}$).

A final comment on dynamic scaling and critical behavior. Usually near critical points, the behavior is determined only by long length scales, the symmetries of the Hamiltonian, and dynamically conserved quantities. In the plaquette model, the short length scales associated with the underlying lattice are relevant even at very small temperatures, as can be seen by the strongly anisotropic behavior of $C_{2,2}(x,y,t)$. However the vanishing of the static correlation function, $C_4^{\rm stat}(x,y)$, away from the axes of the underlying lattice is a result of the symmetries of the Hamiltonian. The similar reduction of $C_{2,2}(x,y,t)$ has its origin in a conserved quantity, namely the number of excited plaquettes in every row and column of the square lattice which is conserved modulo 2. This is the reason for the confinement of dimers to one dimension. The absence of any such conserved quantity in the froth model explains why it is so different from the plaquette model.

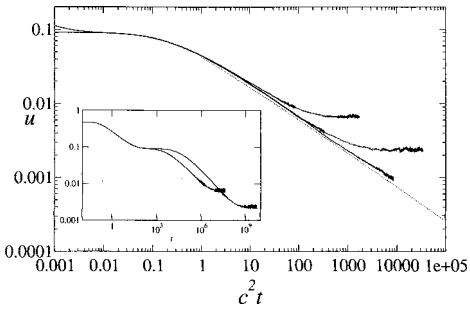

FIG. 10. Time decay of the density of defects, u, after a quench from infinite temperature. (Inset) Data for $\beta=5$ and $\beta=6$. The initial plateau at short times is a signature of the onset of activated dynamics, common to many facilitated spin models. As the density of excited plaquettes falls, the system enters a state in which the vast majority of spins must overcome an energy barrier in order to flip. Thus the dynamics slows down, see [6]. The final plateau is equilibration at a density $(1+e^{\beta})^{-1}$. (Main frame) Quench data from long times, at $\beta=5$, 6, 7; these collapse as a function of rescaled time c^2t, until such time as the system equilibrates. The dotted line is a fit: $A\sqrt{\log(Bc^2t)/(c^2t)}$ with $(A,B)=(0.02,90)$.

C. Suppression of diffusion in the plaquette model

This subtle difference between froth and plaquette models can be made more spectacular when an aging situation is considered. It is known [15] that the aging behavior of the froth model after a quench from high temperature is consistent with diffusion and annihilation of defects, $A+A \to 0$, and has therefore an energy density that decays as $(\log t)/t$ in two dimensions.

In the plaquette model, the conservation of the parity of the number of excitations in each row or column implies that a single defect cannot simply diffuse. Accordingly, we show in Fig. 10 that the aging behavior of the plaquette model is moved out of a simple annihilation-diffusion regime, and the energy density decays much more slowly than $(\log t)/t$. In Ref. [16], we showed that this decay can also be fitted satisfactorily by a power law $t^{-0.45}$ (arising from an decay equation $\partial_t u \propto u^{2.2}$ where we attributed the anomalous exponent to a fluctuation correction). We will argue below that the fluctuation correction is in fact logarithmic; we also note that the same decay was recently fitted on a much smaller time win-

dow as $t^{-1/3}$ [13], invalidated by our simulations performed on much larger time scales.

To explain this behavior, we recall that in two-dimensional annihilation-diffusion processes the effective rate equation is

$$u \sim \frac{\log t}{Dt} + \mathcal{O}(t^{-1}), \tag{24}$$

where $u=\langle H/N+1/2\rangle$ is the density of excited plaquettes, and D is the diffusion constant. In the plaquette model any diffusive step in fact involves movement of at least two excited plaquettes. The simplest such horizontal moves involve isolated excited plaquettes in either the same row, or in adjacent rows, as in Fig. 3, where one isolated defect has moved by emitting a dimer. This pair must then be absorbed by the other isolated excited plaquette, or the system will revert to its original configuration. If the separation of the two isolated excitations is $d \gg 1$ then the probability of the dimer traveling across the gap is approximately d^{-1} [13]. The diffusion constant is therefore proportional to $e^{-2\beta}\langle d^{-1}\rangle$ where the exponential prefactor arises from the activation barrier to dimer creation.

In equilibrium one has $\langle d^{-1}\rangle \sim 1/\xi_2^{\text{stat}} \sim c$. The diffusion constant and inverse relaxation time are both proportional to c^{-3}. Out of equilibrium we should also consider correlations in the density of excited plaquettes. However these correlations take place on a length scale $\approx u^{-1/2}$, which is much smaller than the likely values of d. Therefore we neglect these fluctuations to get $D \propto u$. Substituting into Eq. (24), we find that

$$u \sim \sqrt{\frac{\log t}{t}}. \tag{25}$$

This prediction is in reasonable agreement with Fig. 10. However very many decades of time would be necessary to confirm beyond any doubts this particular form of logarithmic corrections.

D. Dynamical correlations in the froth model

Having described the dynamical correlations of the plaquette model in some detail, we can understand the correlations in the froth model rather easily. There is no restriction on defect concentration in rows and columns of the hexagonal lattice, so the anisotropic behavior of the plaquette model is absent. However the phenomenology is a simple generalization of the behavior described above.

In the absence of spin degrees of freedom, we consider the persistence function $b_{ij}(t,t')$ instead of the autocorrelation function as a local dynamical function. That is, we define

$$C'_{2,2}(x,y,t) = \frac{\langle b_{ij}(t,t_0)b_{i+x,j+y}(t,t_0)\rangle - \langle b_{ij}(t,t_0)\rangle^2}{\langle b_{ij}(t,t_0)\rangle - \langle b_{ij}(t,t_0)\rangle^2}, \tag{26}$$

where the prime indicates that we deal with persistence rather than autocorrelation functions. In the plaquette model, the scaling of $C'_{2,2}(x,y,t)$ is very similar to that of $C_{2,2}(x,y,t)$, compare Figs. 5 and 6. Therefore it is sensible to compare $C'_{2,2}$ for the froth model with $C_{2,2}$ for the plaquette model. Further, since we will find $C'_{2,2}$ to be isotropic for all but the smallest length scales in the froth model, we write its circular average as $C'_{2,2}(r,t)$ and use this latter correlation function in what follows.

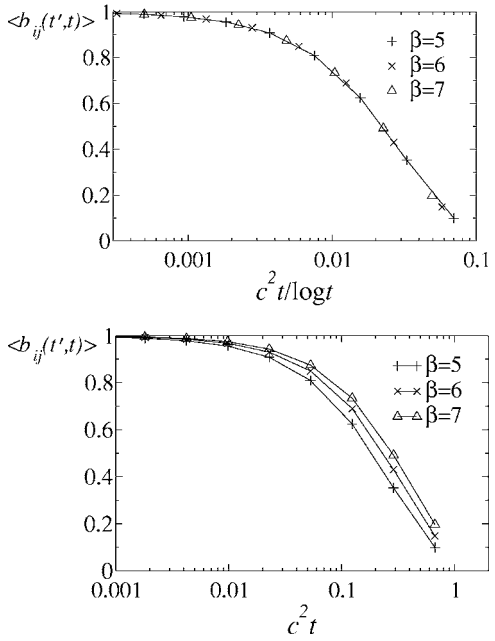

FIG. 11. Two scaling plots of the persistence function in the froth model, showing the effect of logarithmic corrections in two dimensions

To generalize the arguments of Sec. III B to the froth model, we first recall that for random walkers in two dimensions, the typical distance traveled in time t scales as $t^{1/2}$, but the typical number of sites visited by the walker scales as $t/\log t$. Logarithmic corrections arise because $d=2$ is a marginal dimension for free random walks, see Ref. [27] and references therein.

We expect therefore the following generalization of the three regimes observed in the plaquette model. At small times we expect the length scale to grow as $\xi'_{2,2} \sim t^{1/2}$ and the susceptibility to grow with the number of visited sites, $\chi'_{2,2} \sim t/\log t$. Saturation occurs at a length scale controlled by the mean free path of diffusing dimers, which scales as $c^{-1/2}$ and represents the separation of free excitations which absorb the dimers. We note that this length scale is smaller than the mean free path of the plaquette model, which was the typical separation between single defects in the same row or column of the square lattice. Since the scaling is diffusive, saturation will occur at a time, $\tau'_{\text{sat}}/\log \tau'_{\text{sat}} \sim c^{-1}$. The decay of the susceptibility will finally be controlled by the decay of the persistence function on a time scale given by $\tau/\log \tau \sim c^{-2}$.

To illustrate these predictions, we first show the persistence function in Fig. 11, plotted as a function of the naively rescaled variable c^2t, and also against the more appropriate variable $c^2t/\log t$. Since we work over only a few decades of time, we may also obtain reasonable fit to a form $c^{\delta}t$, but the logarithmically corrected variable which has no free parameters appears indeed as the appropriate one.

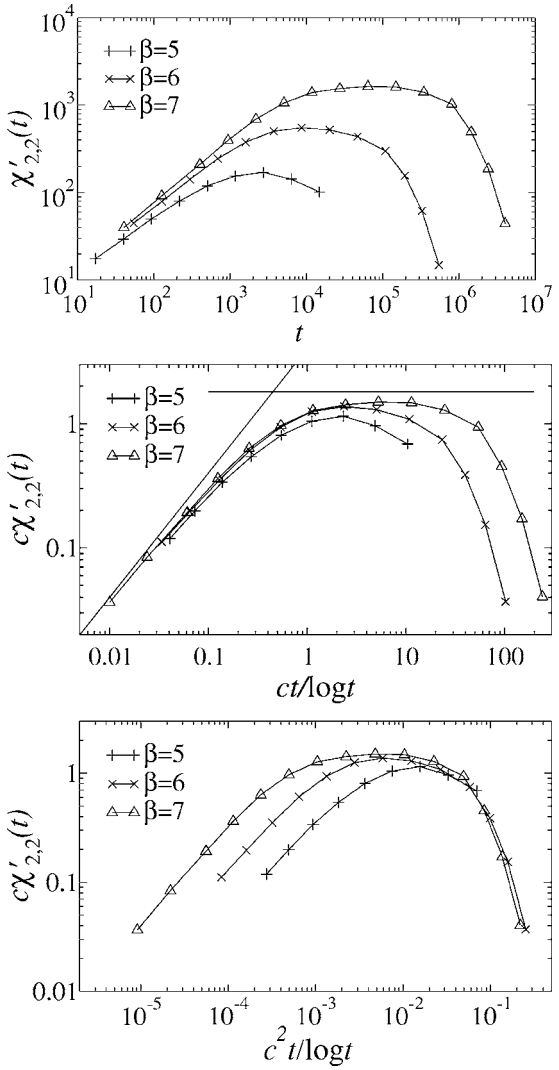

FIG. 12. Top, plots of $\chi'_{2,2}(t)$ at various temperatures. Middle, rescaling of time to $ct/\log t$ showing saturation at $c\tau_{\rm sat}/\log \tau_{\rm sat} \sim 1$. Lines are the random walk prediction $\sim t/\log t$ and a horizontal plateau showing saturation at $c\chi'_{2,2} \sim 1.8$. Bottom, rescaling of time to $c^2 t/\log t$ showing decrease of correlations which scales as the persistence function in Fig. 11.

In Fig. 12 we show the susceptibility associated with the persistence function

$$\chi'_{2,2}(t) = \sum_{xy} C'_{2,2}(x,y,t). \tag{27}$$

Saturation takes place at a value of $\chi'_{2,2}$ that is proportional to c^{-1} and the approach to saturation is a universal function of $ct/\log t$. The susceptibility then decays on the time scale of the persistence function.

The collapse of the persistence and of the susceptibility with a single rescaled time variable is consistent with their dependence on the number of sites visited by each random walker. When considering spatial correlations, the situation is slightly more complicated. While the relevant areas scale as $t/\log t$, the distances traveled by walkers are distributed as universal functions of r^2/t. We therefore expect that while

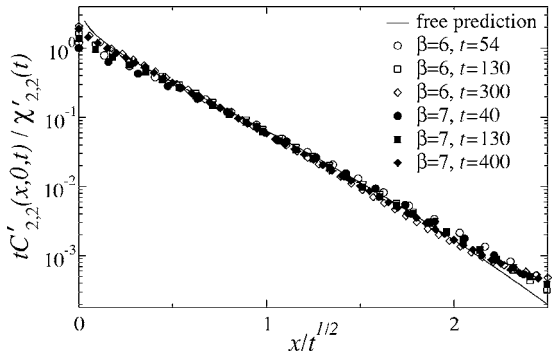

FIG. 13. Scaling plot of $(tC'_{2,2}/\chi'_{2,2})$ as a function of the reduced variable r^2/t. The full line is the independent random walk prediction (31) derived in Ref. [27]. The fit is valid for $r \gg 1$ so the deviations at small r are greatest at small t. The deviations at large r are of the order of the numerical uncertainty in our simulations, but might also be an effect of the zig-zag motion of the dimers.

the susceptibility varies as a scaling function of $t/\log t$, the moments of the probability distribution should have a normal diffusive behavior. That is, we expect

$$\chi'_{2,2}(t) = \int 2\pi r dr\, C'_{2,2}(r,t) \sim t/\log t, \tag{28}$$

but simultaneously

$$\frac{\int 2\pi r dr\, r^n C'_{2,2}(r,t)}{\int 2\pi r dr\, C'_{2,2}(r,t)} \sim t^{n/2}. \tag{29}$$

These relations were proved recently in Ref. [27] for noninteracting random walkers in two dimensions and unnormalized dynamic spatial correlators. An alternative statement of Eq. (29) is that

$$C'_{2,2}(r,t) = \frac{\chi'_{2,2}(t)}{t} f_3\left(\frac{r^2}{t}\right), \quad t \ll \tau_{\rm sat}, \tag{30}$$

which should be valid for $r \gg 1$. This scaling relation must break down at small distance since both $C'_{2,2}(0,t)$ and $\chi'_{2,2}(t)$ are scaling functions of $t/\log t$, incompatible with (30).

We test the collapse of Eq. (30) in Fig. 13. There are tiny deviations at small r^2/t as expected. Moreover we get reasonable agreement with the analytical results of Ref. [27] which predict

$$\frac{tC'_{2,2}(r,t)}{\chi'_{2,2}(t)} = \frac{1}{2\pi D}\int_1^\infty dx \left(\frac{1}{x} - \frac{1}{x^2}\right) e^{-xr^2/2Dt}, \tag{31}$$

where D is the diffusion constant of the random walkers. The diffusion constant for dimers in the froth model will be of order unity since the moves carry no energy penalty. In Fig. 13 we show reasonable fit with $D=1$. We note that the dimers diffuse in a zig-zag fashion. A given dimer makes

random steps of length unity along two nonorthogonal directions that depend on the relative position of the two defects that form the dimer (this orientation is constant as the dimer diffuses). This zig-zag motion will lead to a reduction in the diffusion constant. Since there are only three possible dimer orientations, there is also the possibility of anisotropy in the correlations, but this was not observed in our simulations. Since the scaling of Fig. 13 is good and the fit reasonable, we do not attempt any more rigorous analysis of these effects.

Finally we consider the behavior of the dynamic length scale at saturation. The number of sites visited by a walker increases as $(t/\log t)$. Since the absorbing sites are uniformly distributed the walker will be absorbed on a time scale satisfying $\tau_{\rm sat} \sim c^{-1} \log \tau_{\rm sat}$. In that time the walker travels an average distance

$$\xi_{\rm sat} \sim \tau_{\rm sat}^{1/2} \sim c^{-1/2}[\log c^{-1} + \mathcal{O}(\log\log c^{-1})]^{1/2}. \quad (32)$$

In Fig. 13 (top) we present scaling of the saturated correlation function according to this law. We also show in Fig. 13 (bottom) that when times become of the order of or larger than the persistence time, the change in the susceptibility $\chi'_{2,2}(t)$ is mainly due to a change in the strength of the correlations while the dynamic length scale $\xi'_{2,2}$ is approximately constant, just as in the plaquette model. We attribute the weak decrease of the correlation length at the longest times to the fact that the persistence function retains rather little information for times much greater than the relaxation times τ. As a consequence the free random walk calculations in Ref. [27] do not apply at large times because they do not take saturation effects into account.

To summarize the results of this section, we have shown that the froth model behaves similarly to the plaquette model with a mean free path for dimers that scales as $c^{-1/2}$ and a relaxation time scale that scales as c^{-2} with important logarithmic corrections due to the dimensionality of the random walks performed by freely diffusing dimers.

IV. CONCLUSION

The plaquette model is a spin model with simple dynamics and no finite temperature thermodynamic singularities. Its Hamiltonian gives rise to effective kinetic constraints, and therefore to dynamical heterogeneity. Despite simple thermodynamics in the plaquette representation, spins have static correlations whose length scales diverge at low temperature. The symmetries of the Hamiltonian mean that only rather specific correlation functions have nonzero expectations. However, measurement of the fluctuations in two-point quantities allow extraction of the relevant length scales.

Spatial correlations are strongly anisotropic. For static correlations, this is the result of a symmetry of the spin system. Dynamical correlations are anisotropic because of a microscopic conservation law. We have identified three length scales in the plaquette model. The mean spacing between excited plaquettes, $\xi_4^{\rm stat} \sim c^{-1/2}$ controls four-point static correlations. Fluctuations in two-point structure factors are controlled by $\xi_2^{\rm stat} \sim c^{-1}$ which represents the mean distance between adjacent excited plaquettes in the same row or column. Finally there is a dynamical length scale $\xi_{2,2}(t)$ whose behavior is diffusive at small times and saturates to $\xi_2^{\rm stat}$ at larger times.

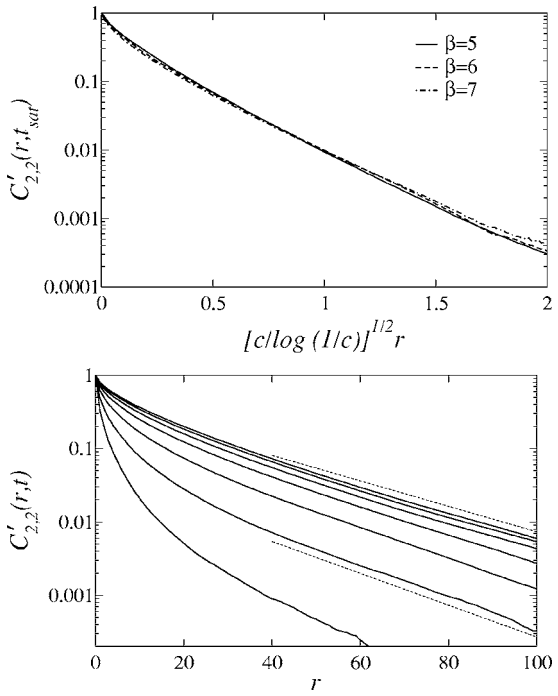

FIG. 14. Top, plot of $C'_{2,2}$ in the state with a saturated correlation area showing good scaling as a function of $r\sqrt{c\log(1/c)}$. Bottom, plot of $C'_{2,2}(r)$ at logarithmically spaced times between 0.3τ and 10τ, with β=7. As time increases, the strength of the correlations decreases by two orders of magnitude. On the other hand, the gradient of these traces at large distances gives the correlation length which is decreasing rather slowly with time (we show dashed lines marking $e^{-r/25}$ and $e^{-r/20}$). We constrast this behavior with the unsaturated regime in which the correlations are always strong, and the correlation length *increases* as $t^{1/2}$.

We also identified two time scales in the system. The first is the saturation time, $\tau_{\rm sat} \sim c^{-2}$, which separates the regime in which dynamical correlations have an increasing length scale from the regime in which their length scale is saturated. The second is the relaxation time $\tau \sim c^{-3}$ which represents the typical time for the spin field to lose the memory of its initial configuration. This separation of time scales arises from the nontrivial conserved quantities at the zero temperature dynamical fixed point. We also showed that these effects lead to unusual aging behavior.

We explained the dynamical length and time scales in the plaquette model in terms of diffusion of excitation pairs along one-dimensional paths. We showed that the froth model correlations are obtained by generalizing these results to allow the excitation pairs to diffuse in two dimensions. This introduces logarithmic correlations, but once these have been taken into account the scaling is as expected for noninteracting random walkers.

The results connecting static and dynamic correlations in the plaquette model demonstrate one specific mechanism by which a mobility field emerges from a more familiar

interacting spin field. They are relevant to the description of structural glasses in these terms. The fact that all of the dynamical correlations can be explained in terms of independent random walkers provides further evidence that this behavior is rather universal in systems with dilute diffusing defects.

ACKNOWLEDGMENTS

The authors thank G. Biroli and C. Toninelli for discussions. This work was supported by CNRS (France), EPSRC Grants No. GR/R83712/01 and GR/S54074/01, and University of Nottingham Grant No. FEF 3024.

[1] J. P. Garrahan and D. Chandler, Phys. Rev. Lett. **89**, 035704 (2002); Proc. Natl. Acad. Sci. U.S.A. **100**, 9710 (2003).
[2] L. Berthier and J. P. Garrahan, J. Chem. Phys. **119**, 4367 (2003); Phys. Rev. E **68**, 041201 (2003); J. Phys. Chem. B **109**, 3578 (2005).
[3] S. Whitelam and J. P. Garrahan, J. Phys. Chem. B **108**, 6611 (2004).
[4] G. H. Fredrickson and H. C. Andersen, Phys. Rev. Lett. **53**, 1244 (1984).
[5] J. Jäckle and S. Eisinger, Z. Phys. B: Condens. Matter **84**, 115 (1991).
[6] F. Ritort and P. Sollich, Adv. Phys. **52**, 219 (2003).
[7] S. Whitelam, L. Berthier, and J. P. Garrahan, Phys. Rev. Lett. **92**, 185705 (2004); Phys. Rev. E **71**, 026128 (2005).
[8] S. Whitelam and J. P. Garrahan, Phys. Rev. E **70**, 046129 (2004).
[9] L. Berthier, Proc. SPIE **5469**, 177 (2004).
[10] A. Lipowski, J. Phys. A **30**, 7365 (1997).
[11] J. P. Garrahan, J. Phys.: Condens. Matter **14**, 1571 (2002).
[12] A. Buhot and J. P. Garrahan, Phys. Rev. Lett. **88**, 225702 (2002).
[13] D. Espriu and A. Prats, Phys. Rev. E **70**, 046117 (2004).
[14] C. A. Angell, Science **267**, 1924 (1995).
[15] L. Davison and D. Sherrington, J. Phys. A **33**, 8615 (2000); T. Aste and D. Sherrington, *ibid.* **32**, 7049 (1999).
[16] R. L. Jack, J. P. Garrahan, and D. Sherrington, Phys. Rev. E **71**, 036112 (2005).
[17] R. J. Baxter, *Exactly Solved Models in Statistical Mechanics* (Academic, London, 1982).
[18] X. Xia and P. G. Wolynes, Proc. Natl. Acad. Sci. U.S.A. **97**, 2990 (2000).
[19] D. Kivelson, S. A. Kivelson, X. L. Zhao, Z. Nussinov, and G. Tarjus, Physica A **219**, 27 (1995).
[20] M. Mézard and G. Parisi, Phys. Rev. Lett. **82**, 747 (1999).
[21] E. Bertin, cond-mat/0410537 (unpublished).
[22] F. H. Stillinger and T. A. Weber, Science **267**, 1935 (1995).
[23] J. P. Bouchaud and G. Biroli, J. Chem. Phys. **121**, 7347 (2004).
[24] M. E. J. Newman and G. T. Barkema, *Monte Carlo Methods in Statistical Physics* (Oxford University Press, Oxford, 1999).
[25] S. C. Glotzer, J. Non-Cryst. Solids **274**, 342 (2000).
[26] P. Mayer, H. Bissig, L. Berthier, L. Cipelletti, J. P. Garrahan, P. Sollich, and V. Trappe, Phys. Rev. Lett. **93**, 115701 (2004).
[27] C. Toninelli, M. Wyart, L. Berthier, G. Biroli, and J. P. Bouchaud, Phys. Rev. E (to be published).